Full Scale Dynamic Testing of Large Area Suspended Ceiling System

K.P. Ryu, A.M. Reinhorn & A. Filiatrault
University at Buffalo, USA

SUMMARY:
A series of experiments to investigate the seismic behavior of large area suspended ceiling systems were performed using a tandem of shake tables at UB-SEESL in USA. For the full scale dynamic testing, a new test frame providing a continuous ceiling area of 6.1 m × 16.3 m (100 m^2) was constructed on the shake tables and was equipped with an open loop compensation procedure for the frame corrections. Fifteen test configurations were selected in order to determine the effects or efficiency of ceilings parameters. Based on the test data and the failure mechanisms observed, fragility curves are developed. Simplified analytical models are developed to represent the mechanics of the tested systems. The paper presents the experimental study, the unique control systems, the basic lessons learned from the experiments, and the development of simple computational tools to predict the design forces required for achieving a safe ceiling construction within the expected seismic ranges.

Keywords: nonstructural components; shake table experiments; open-loop compensation

1. TEST OBJECTIVES

Full scale shake table tests of suspended ceiling systems were conducted in order to evaluate the response of the systems subjected to earthquake induced excitation. The main objectives of this study are (1) identify failure mechanisms, which describe functionality (limit states) of the system, (2) investigate the effects and efficiency of various systems, required by the current standard ASTM E580 for seismic design, and the influence of installation conditions, and (3) develop computational tools to determine element forces to provide better understanding of their seismic design.

2. SET UP & CONFIGURATION

A new steel test frame of 6.3m × 16.5m was constructed for the full scale dynamic testing on the tandem six *degrees-of-freedom* (DOF) shake tables at the Structural Engineering and Earthquake Simulation laboratory (SEESL) at the University at Buffalo (UB), shown in Figure 2.1 (left). The test frame consisted of 3 modular segments: two 6.3m×6.3m square frames, and a 3.9m×6.3m link frame.

Figure 2.1. New test frame: 6.3m×16.5m large test set up (left) and 6.3m×6.3m small test set up (right)

The two square frames were respectively mounted on each of two 7m × 7m shake table extensions. A 3.2m × 7.0m bridge structure was installed as a work surface between the two extensions. Open web steel joists were used for the roof grid system in combination with steel tube bars to form 1.2m × 1.2m modules. In order to install the 100 m^2 continuous ceiling system, two stiffer open side walls, having no inside columns and braces, were installed in the middle of the frame. Further details on the design of the test frame can be found in Reinhorn *et al*. (2010). In order to investigate the effects of a ceiling system area size, smaller area tests were also conducted using one of two square frames as shown in Fig 2.1 (right).

The dynamic properties of the bare frame and the frame with the installation of typical ceiling system (tile weight = 1.05psf) were identified using transfer functions calculated from acceleration histories, between the shake table extension and the roof center of the test frame, achieved from white noise tests (range of 0.1hz to 50hz). The results are presented in Table 2.1. With the installation of a suspended ceiling system the fundamental frequency of the frame slightly increased.

Table 2.1. Characteristic frequencies (in Hz) of test frames, before and after ceiling system installation

Direction	6.3m × 16.5m frame		6.3m × 6.3m frame	
	Bare	Ceiling installed	Bare	Ceiling installed
1	*2*	*3*	*4*	*5*
Longitudinal (x)	13.3	13.8	12.0	13.3
Transverse (y)	11.3	12.0	12.8	13.3
Vertical (z)	22.0	23.3	21.8	23.0

The long side (16.5m) and the short side (6.3m) of the frame are denoted as the longitudinal direction (x, east-west) and the transverse direction (y, north-south), respectively. Main runners were installed along the longitudinal direction for all test configurations. In order to measure the response of the test system, total 133 instruments including 82 accelerometers, 20 load cells, 16 displacement transducers, and 15 spring potentiometers were installed to the shake table extension, the test frame, and ceiling systems (i.e. specified main runners, cross tees, hanging wires, and ceiling tiles).

A total of fifteen different test configurations were tested to investigate the addressed test objectives. The test descriptions of ten tests performed on the 6.3m × 16.5m frame and five tests performed on the 6.3m × 6.3m frame are summarized in Table 2.2. Test #1 was used for the calibration of the equipment, tuning the motions for the ceilings, and testing the influence of variation of vertical input effects. The ceiling system failed prematurely in the low level test, probably caused by the influence of the multiple preparation tests. The result is reported for completion, but since it was repeated in test #4, it is not considered in further evaluation process. Test #2, #3, and #4 were conducted to investigate the effects of multi directional input motions as indicated in the column 3 and 12 of Table 2.1. For all tests except Test #2 and #3, three directional input motions were used. Test #5 set up was the same as the one of Test #4 but without lateral restraints. For Test #6, heavy tiles (4.00psf) were used instead of 1.05psf. Test #7 was performed to compare the response of a ceiling system where seismic clips were connected to 7/8 inch wall angles and without lateral restraints to the response of a grid with pop rivets conneted to 2 inch wall angles (as installed for Test #4) with lateral restraints. Test #8 was focussed on a setup of non-seismic design – intermediate weight grid for SDC C. Test #9 set up was the same as the one of Test #4 except that larger light fixtures (0.6m × 1.2m) were installed in the transverse direction. Finally, Test #10 was performed to investigate the effects of deep plenum height (1.6m from the bottom of joists to the ceiling level, comparing to 0.7m of all the other test configurations). Test #11 through #15 were condcuted to investigate the effects of size of ceiling areas, i.e. 6.1x6.1, 4.9x4.9, and 3.7x3.7m; Test #11, #13, #15 had the same configuration as the one of Test #7, and Test #12 and #14 configurations were the same as the one of Test #4 as described in Table 2.2.

Test input motions in the x, y and z directions, representing floor acceleration histories induced during seismic events, were generated using an accelerogram simulation program in STEX (MTS, 2004) to match the *roof required response spectrum* (RRS) according to the AC156 standard for shake table testing of nonstructural components (ICC, 2010). The desired (or target) motions are intended to be

generated at the roof level of the frame where the suspended ceiling system is installed. However, since the test frame has its flexibility and a test system is not perfect, a compensation procedure is required to generate the target motion at the desired roof location.

The intensity of RRS is defined using the mapped maximum earthquake spectral accelerations at short periods S_s. Each test configuration was subjected to incremental input motions, starting from S_s = 0.50g and increased by ~0.25g until the celing system collapsed, after which the tests were ceased and a new celing system was installed. The collapse level of a tested ceiling system in this study was defined as the level of the test, at which the number of fallen tiles or damaged grid members exceeded more than 10% of the total number of each component. Column 4, 5, and 6 of Table 2.2 present the collapse level of each test series in terms of target or achieved input motion intensity in the horizontal direction: FA_H in column 5 is the target horizontal peak floor acceleration and calculated from S_s as $FA_H = 0.8 \times S_s$, which represents the zero period acceleration (ICC, 2010). PFA_H in column 6 is the achievd peak floor acceleration at the roof center of the 6.3m × 6.3m squre frame (for the large area tests, the average of two roof center peak accelerations). PFA_H is the compensated achieved motion through the compensation procedure.

Table 2.2. Test Description

#	Size ($m^{2)}$	Input	Collapse Level (g)			Grid Duty	Panel Weight (psf)	Lateral restraint	Peri. angle	Plenum Height	Comments
			Target S_S^2	Target FA_H^3	Achieved PFA_H^4						
1	*2*	*3*	*4*	*5*	*6*	*7*	*8*	*9*	*10*	*11*	*12*
Performed on 6.3m × 16.5m test frame											
1	6.1×16.3	3D	-	-	-	Heavy	1.05	Yes	2”	29”	Early Failure
2	6.1×16.3	x, z	2.75	2.20	2.52	Heavy	1.05	Yes	2”	29”	2D effect
3	6.1×16.3	x	2.75	2.20	2.09	Heavy	1.05	Yes	2”	29”	1D effect
4	6.1×16.3	3D	2.25	1.80	1.52	Heavy	1.05	Yes	2”	29”	3D effect
5	6.1×16.3	3D	2.00	1.60	1.26	Heavy	1.05	No	2”	29”	No restraints
6	6.1×16.3	3D	1.50	1.20	1.06	Heavy	4.00	Yes	2”	29”	Heavy panel
7	6.1×16.3	3D	2.25	1.80	1.49	Heavy	1.05	No	7/8”+clip	29”	Seismic clip
8	6.1×16.3	3D	1.75	1.40	1.12	Interm-ediate	1.05	No	7/8”	29”	SDC C – All free ends
9	6.1×16.3	3D	2.75	2.20	1.95	Heavy	1.05	Yes	2”	29”	2×4 Light fixture
10	6.1×16.3	3D	2.50	2.00	1.87	Heavy	1.05	Yes	7/8”+clip	65”	Deep plenum
Performed on 6.3m × 6.3m test frame											
11	6.1×6.1	3D	2.25	1.80	1.54	Heavy	1.05	No	7/8”+clip	29”	vs. Test#7
12	6.1×6.1	3D	2.75	2.20	2.02	Heavy	1.05	Yes	2”	29”	vs. Test#4
13	4.9×4.9	3D	2.75	2.20	1.99	Heavy	1.05	No	7/8”+clip	29”	vs. Test#7
14	4.9×4.9	3D	2.75	2.20	1.95	Heavy	1.05	Yes	2”	29”	vs. Test#4
15	3.7×3.7	3D	3.25	2.60	2.65	Heavy	1.05	No	7/8”+clip	29”	vs. Test#7

3.OPEN LOOP COMPENSATION

Due to the dynamics of a test frame and the shake table, the frame cannot deliver accurately a target floor motion at a desired location when the motion is applied at the level of the shake table. A compensation procedure can provide a compensated command drive signal to the shake table in order to obtain an acceptable reproduction of the target motion at a specific location of the frame. The distortions in signal reproduction due to the imperfect shake table system and the frame structure dynamics are respectively represented by transfer functions H_t and H_s in the frequecy domain:

$$H_t = \frac{achieved\ table\ motion}{desired\ table\ motion}, \quad H_s = \frac{achieved\ structure\ motion}{achieved\ table\ motion} \tag{3.1}$$

The transfer function of the whole system can be explained:

$$H = \frac{achieved\ structure\ motion}{desired\ table\ motion} = \frac{y_s}{x_{desire}} \tag{3.2}$$

In order to obtain the best fidelity of the achieved structure motion, a compensated new drive motion $x_{c\text{-}drive}$ can be applied as shown in the following equation:

$$if \quad x_{c-drive} = H^{-1}x_{desire} \quad then \quad y_s = Hx_{c-drive} = HH^{-1}x_{desire} \cong x_{desire} \tag{3.3}$$

where H^1 is the inverse transfer function of the table-structure system. Due to the nonlinearity of the system, the achieved motion can not match perfectly the desired motion so that an iteration is required if the error ($\varepsilon = x_{desire} - y_s$) is larger than a defined tolerance. Further details on this compensation procedure can be found in Maddaloni *et al*. (2010).

This concept was implemented for these series of tests and perforemd at the beginning of each configuration test since a different set up could affect the response of the system, resulting in a different transfer function. The compensation results are shown in Figure 3.1 including the response spectra of the RRS for S_s = 0.5g, the desired motion (x_{desire} = Target) derived from the RRS, the uncompensated achieved structure motion (ACH-U), the compensated drive motion ($x_{c\text{-}drive}$ = DES-C), and the compensated achieved structure motion (ACH-C) at the roof center of the 6.3m × 6.3m square test frame (i.e. the compensation results of each square frame of the large frame were very similar).

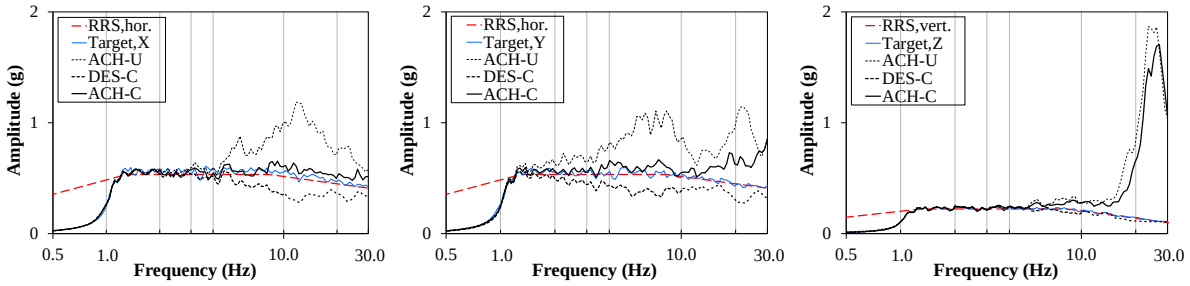

(a) longitudinal (b) lateral (c) vertical

Figure 3.1. Comparison of required (RRS), desired (Target), uncompensated achieved (ACH-U), compensated drive (DES-C), and compensated achieved (ACH-C) spectra

It is clear that the compensated achieved motion at the specific location matches quite well the desired motion obtained from the RRS in the horizontal directions. In the vertical direction the compensated achieved motion did not agree the desired motion in the range of 15hz to 30hz. The discrepancy was caused by the roof resonance at its fundamental frequncy of 23hz, which represents the one of a concrete slab (5-7in. thickness) having the same area (Blevins, 1979). The resonance could be reduced by an energy dissipating system (i.e. damper) or could be controlled to represent more flexible floor system by adding mass on the roof structure. This resonance at the center of a floor structure is realistic and shall be included in a suspended ceiling dynamic test. To challenge the system to maximum response for a flexible structure, it was recommended that a frame roof vertical frequncy be in the range of 2.6hz to 8hz, which is the flat portion of the RRS (Reinhorn *et al*., 2010).

4.TEST RESULTS

General observations related to system failure mechanisms are presented in this section. Based on the failure mechanisms, limit states were defined and fragility curves were developed for each test configuration. The results are compared in order to investigate the effects of design parameters.

4.1 General observations

The dynamic forces in the longitudinal direction were collected by main runners from a tributary area of 1.2 m and transmitted to the end of the runners or to lateral restraints (splay wires). Early failure of pop rivets (perimeter connections to wall angles) occurred at the end of unrestrained main runners and cross tees when the collected forces exceeded the shear strength of a pop rivet and resulted in large displacement of a main runner. This failure can be considered as *repairable damage* since the unattached main runner can be reconnected to a wall angle using a new rivet at a new hole.

The lateral restraints in the longitudinal direction acted to reduce horizontal movements of the restrained main runners only. No grid components provided enough lateral stiffness to transfer tributary loads from unrestrained runners to the one supported by the restraints. The lateral restraints prevented severe bending in the transverse direction of the *restrained main runners* by acting as the supports of a continuous beam. However, the *unrestrained main runners* deflected more substantially due to their longer unrestrained span.

Another failure mechanism occurred at the connections of cross tees. It was observed that the end clip of cross tees was pulled out when element forces at the connection exceeded the capacity of the end clip. At this failure mode, the cross tees were not damaged, except for their connecting tabs. In the longitudinal direction 0.6m cross tee connection failed when the displacement of the adjacent main runners increased due to pop rivet failure or strong excitations. In the transverse direction 1.2m cross tee connections were disconnected due to the large transverse deflection of main runners at the free side (floating side) or between the lateral restraints. This grid connection failure can be repairable if the number of damaged grid connections is limited and the failure is localized. When the number of damaged connections increases, the repair effort can be significant since grid failures result in the misalignment of the total system, and large area grid adjustments will be required.

After grid connections failed, a massive dislocation of ceiling tiles followed. The grid connection failure and the loss of adjacent tiles allowed the increase of deflection of grid components, which were supported by the failed grid and tiles, and resulted in further dislocation of ceiling tiles and also additional grid failure. "Domino effect" on failure occurred due to the substantial movement of large area of mass toward to the unsupported part of the system.

The collapse of a suspended *ceiling system* can be defined as the exceedance of the specific percentage of a damaged system, which can be defined by the ratio between the number of damaged components and the total number of components. In this study, a collapse limit state was defined as the failure of the 10% of the number of total gird elements, or ceiling tiles. When the collapse occurred, all the components of the tested system were replaced with new ones, except ceiling tiles, light fixtures and diffusers, which were reused, if those had minor damage.

4.2. Preliminary result analysis

Fragility analysis was performed in order to investigate the effects of installation conditions. The probability P_f of reaching or exceeding the limit states is defined as (Badillo *et. al*, 2007):

$$P_f = N_f/N \tag{4.1}$$

where N_f is the number of fallen tiles or failed cross tee connections (if one of two end connections of a cross tee failed, the cross tee was counted as a failed one), and N is the total number of ceiling tiles, or the total number of cross tees defining the limit state. Based on the failure mechanisms observed during the experiments, two limit states indicating the collapse of a system were defined as: (1) the loss of 10% of ceiling tiles (N = 10% of total tiles) and (2) the failure of 10% of grid components (cross tee connection failure) (N = 10% of grid components). Other limit states could be chosen based on the experimental data, which is available in NEES repository in the US.

Two fragility curves were developed per each test configuration, as shown in Figure 4.1, as a function of the *peak floor acceleration* (PFA) achieved at the center of test frame's roof using the two limit states defined above. The smoothed curve of Figure 4.1 was generated using the standard log-normal cumulative distribution function to match the experimental data, which are identified using symbols.

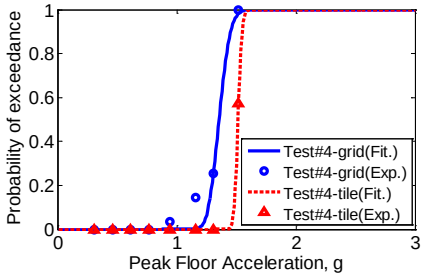

Figure 4.1. Fragility curves for Test #4

The fragility curves show that in most cases the grid failure provides a lower limit state of damage than the fallen tiles (i.e. a grid system failed before ceiling tiles fell.) in this configuration. However, the fragility curves of some configurations crossed each other, showing that the two limit states are not absolutely dependent. Fragility curves were used to differentiate quantitatively the effects of parameters as shown in Figure 4.2, based on the fragility using the limit state of a grid failure.

For the defined limit states, based on median probability, it was found that (1) a ceiling system subjected to three directional input is more vulnerable than the one excited by one or two directional motions, (2) the ceiling system having heavier weights is a more vulnerable system, (3) the seismic performance of the ceiling system is improved with the installation of lateral restraints, and (4) The ceiling system having larger system area size is more vulnerable than the system of smaller size.

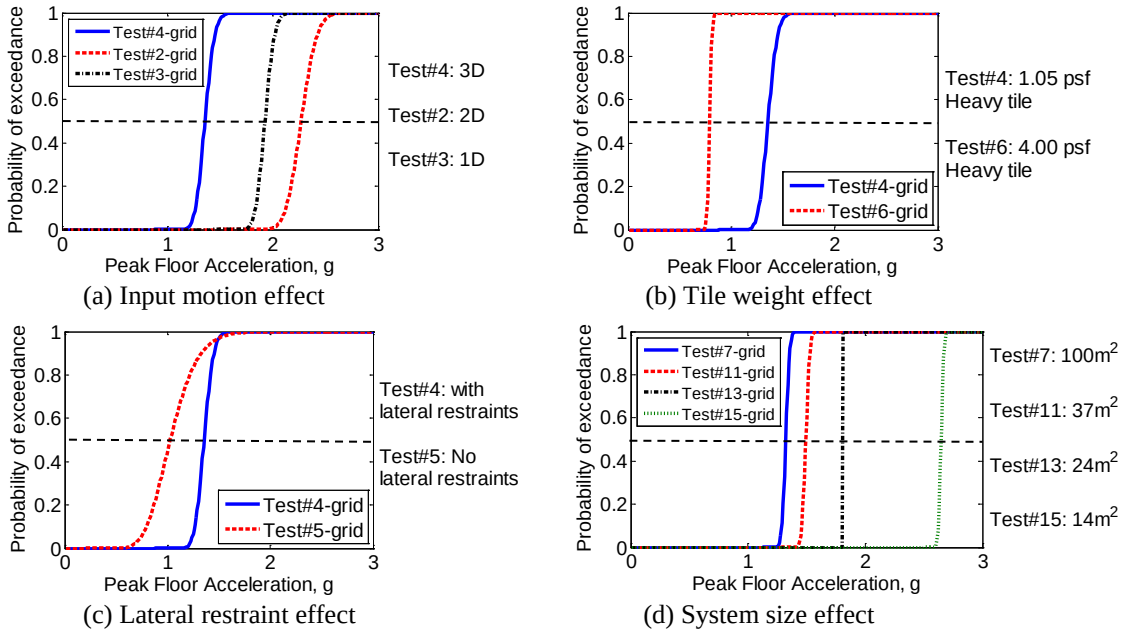

Figure 4.2. Fragility curves for the limit state of a grid failure

5. ANALYTICAL MODELS

Using on the test observations and measured responses, simplified uni-directional analytical models are developed in order to understand the response of the system subjected to external excitations. The results of the analytical models are compared with the measured responses from experiments.

5.1. System analysis in the longitudinal direction

As described in the previous section, inertia forces induced by external excitation are collected in the longitudinal direction by main runners and the forces are transmitted to end connections such as pop-rivets of a fixed side wall. In the longitudinal direction the suspended ceiling system can be considered as a multi-pendulum system interconnected by slip-lock springs k_{gr}, representing main runner splices. The ocillation of this sytem is resisted by end connection springs k_{ri} (pop rivet), and after the pop-rivets fail, the motion is restrained by end walls, whose effect can be represented by external force F_{rs}. The horizontal displacement of the system is limited and small compared to the radius of curvature of the pendulum system. Using the small displacement assumption, the lateral stiffness of hanging wires k_w is considered as mg/h (Fenz *et al.*, 2008), where m and h are the lumped mass from a 1.2m tributary area and the height between the ceiling system to a support structure (i.e. plenum height) respectively. The schematic of the system is presented in Figure 5.1.

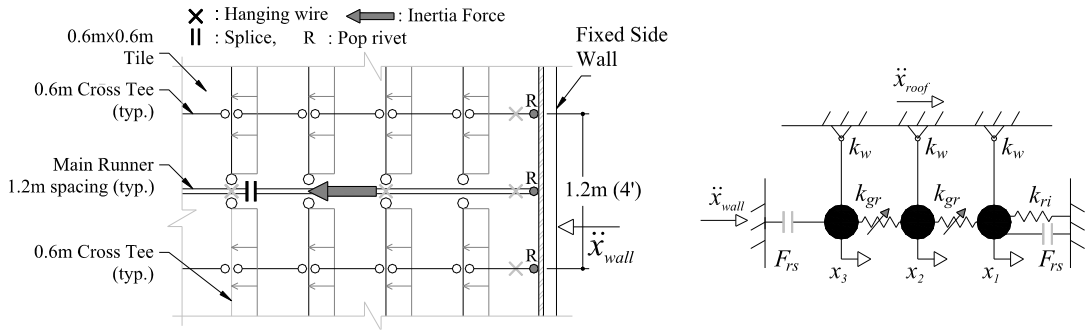

Figure 5.1. The schematic of a suspended ceiling system subjected to longitudinal excitation

The system is subjected to two excitations during seismic events before end connection fails, a floor motion at the roof of the test frame and a ceiling level wall motion, amplified in accordance of the structure dynamics. The wall excitation can be different with the roof excitation due to out of plane vibration of the wall. From the experiments it was observed that the joints of grid members such as the splice of main runners and end clip of cross tees can be modelled as a slip-lock springs to simulate the locking behavior, which occurs when the joint displacement exceeds its slip distance. A *Gaussian Pinching Model* in series with a hysteretic spring suggested by Reinhorn *et al.* (1995) could be used. In this study, the multiple-support excitation and nonlinearity of slip-lock spring are not considered.

The equation of motion for the suspended ceiling system excited in the horizontal excitation is therefore:

$$[M]\{\ddot{x}(t)\}+[C]\{\dot{x}(t)\}+[K]\{x(t)\}+\{F_{rs}\}=-[M]\{I\}\ddot{x}_{wall}(t) \tag{5.1}$$

where $[M]$, $[C]$, $[K]$ are respectively the mass, damping and stiffness matrix, and $\{F_{rs}\}$, $\{I\}$ are the external force vector due to end wall contact, and the influence vector, whose element is unity. For the 3 *degree of freedom* (DOF) system shown in Figure 5.1 (right), the mass and stiffness matrix and the external force vector are:

$$[M]=\begin{bmatrix} m & 0 & 0 \\ 0 & m & 0 \\ 0 & 0 & m \end{bmatrix}, \quad [K]=\begin{bmatrix} k_{gr}+k_{ri}+k_w & -k_{gr} & 0 \\ -k_{gr} & 2k_{gr}+k_w & -k_{gr} \\ 0 & -k_{gr} & k_{gr}+k_w \end{bmatrix}, \quad \{F_{rs}\}=\begin{Bmatrix} F_{rs^+} \\ 0 \\ F_{rs^-} \end{Bmatrix} \tag{5.2}$$

where the mass m is assumed to be discretized at each main runner splice and lumped at the middle of each main runner: it is caculated from the 1.2m tributary area. With the idealized lumped masees the mass matrix is diagonal. At the failure of a pop rivet, the stiffness matrix changes ($K_{11} = k_{gr} + k_w$), and the system is excited by the roof motion. F_{rs+}, F_{rs}- are the additional resisting forces exerted by gap components, which are added in parallel to both end masses to model the stiffening that occurs when

contact is made with each end wall (Fenz, 2008). The additional forces are given by:

$$F_{rs+} = k_{rs}\left(x_1 - d_{rs+}\right)H\left(x_1 - d_{rs+}\right), \qquad F_{rs-} = k_{rs}\left(x_3 + d_{rs-}\right)H\left(-x_3 - d_{rs-}\right) \tag{5.3}$$

where k_{rs} is the stiffness exhibited by an end wall, d_{rs+} and d_{rs}- are the gap displacements between the end of a main runner and the wall, and H is the *Heaviside step function*. The damping matrix $[C]$ is taken as the Rayleigh damping matrix, which is $[C] = a_0[M] + a_1[K]$, where:

$$a_0 = 2\xi\omega_1\omega_2 / (\omega_1 + \omega_2), \quad a_1 = 2\xi\omega_1\omega_2 \tag{5.4}$$

in which ξ is the critical damping ratio, ω_1 and ω_2 are the first and second natural frequencies of the structure. The damping matrix is a constant matrix and changes once when the stiffness matrix changes due to the pop rivet failure; however, if the slip-lock spring was used, the damping matrix should be changed in accordance with the change of the stiffness matrix, only. Eqn. (5.1) can be expressed as a system of first order ordinary differential equations of the form:

$$\{\dot{x}\} = [A]\{x\} + \{B\} \tag{5.5}$$

where the vector $\{x\}$ includes each displacement and velocity of DOFs and the matrix $[A]$ and the vector $\{B\}$ are populated accordingly. In this study, the equation of motion is solved using the *ode15s* solver in MATLAB™ by Matworks Inc. to obtain structural responses.

The new model was used to simulate structural responses of the tested system of Test #4 (6.1m × 16.3m ceiling system) for the test of S_s = 1.5g (PFA = 0.94g). The 3 DOF system of Eqn. (5.1) was extended to the 5 DOF system, representing 5 main runners interconnected by splices. The mass of each main runner tributary area was lumped at the center of each main runner and calculated from 1.2m × 3.3m area: m = 60 lb/g. Parameters were estimated from material properties and other shake table test responses. An equivalent critical damping ratio, ξ = 30%, was estimated from system transfer function. The damping seems large, but due to the loose components and friction in joints, such damping is possible. The wire stiffness $k_w = mg/h$ = 0.0019 kips/in. The pop-rivet spring stiffnes $k_{ri} = f_{ri}/u_{ri} \times \alpha$ = 1.36 kips/in, with the lateral strength of f_{ri} = 0.16 kips, the maximum spring displacement at failure u_{ri} = 0.20 in., and the weighting factor α = 1.70, chosen to consider the contribution of adjacent rivets to the tributary area of one main runner. The grid spring stiffness of k_{gr} = 5.44 kips/in. was calculated from the test records. A stiffness k_{rs} = 100 kips/in. was used for the end wall. The end wall gap displacements d_{rs+} and d_{rs}- were estimated as 0.11 in. and 0.58 in., respectively.

The displacement history at the fixed end of a main runner obtained from the analysis is compared in Figure 5.2 with the measured response from experiments. The force demand exceeded the capacity of a pop-rivet at ~18 sec and the fundamental frequency of the system changed. The discrepancy in the range of 18 sec to 26 sec may be caused by the effects of adjacent cross tee pop rivets, whose failure followed due to the large displacement of the main runner.

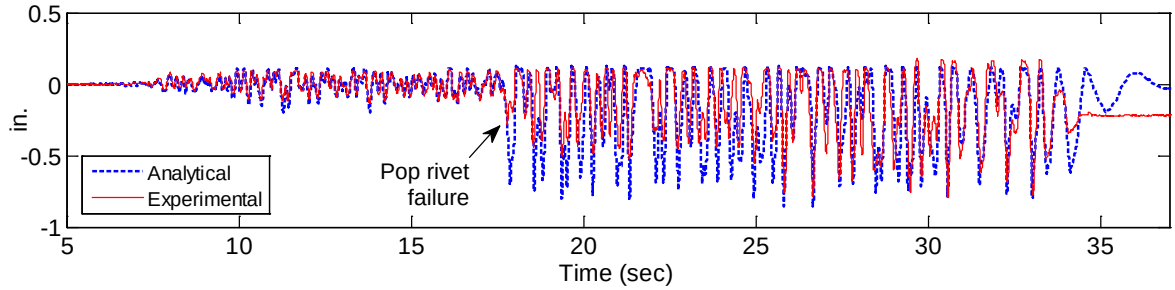

Figure 5.2. Comparison of displacement histories from a seismic test: Test #4, S_s = 1.5g (PFA = 0.94g).

5.2. System analysis in the transverse direction

The suspended ceiling system can be modelled in the transverse direction of main runners as a simply supported beam with additional support springs that represent the horizontal restrainers as shown in Figure 5.3. The beam with end supports and the additional springs represent a main runner with distributed mass (of 1.22 m wide tributary area) including tiles and cross tees, restrained by end connections, lateral restraints, and cross tee and pop-rivet connections, respectively.

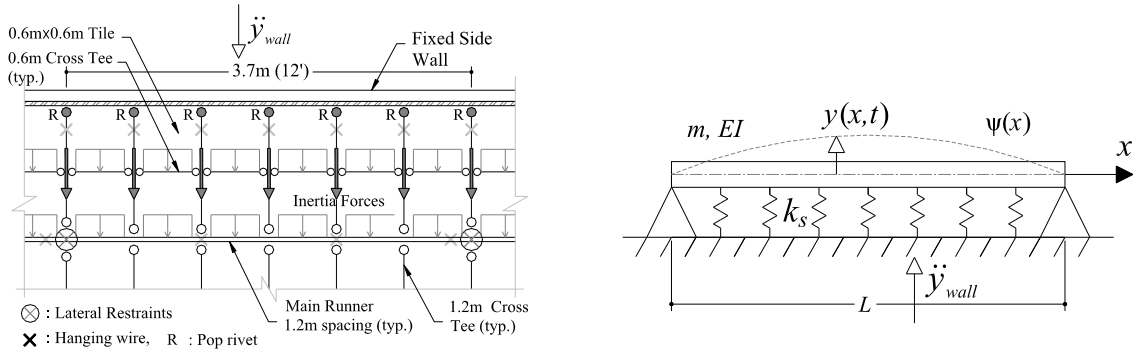

Figure 5.3 The schematic of a suspended ceiling system in the transverse direction

The beam can be considered as a generalized single degree of freedom system, where its deflections $y(x, t)$ can be related to a single generalized displacement $z(t)$ through a shape function $\psi(x)$. The equation of motion can be written (Chopra, 2007)

$$\tilde{m}\ddot{z} + c\dot{z} + \tilde{k}z = -\tilde{L}u_g(t) \tag{5.6}$$

where

$$\tilde{m} = \int_0^L m(x)[\psi(x)]^2 dx, \quad \tilde{k} = \int_0^L EI(x)[\psi''(x)]^2 dx + \sum_{i=1}^{n} k_s[\psi(x_i)]^2, \quad \tilde{L} = \int_0^L m(x)[\psi(x)]dx \tag{5.7}$$

with the constant c being the viscous damping coefficient, and the additional spring stiffness $k_s = k_{ri}k_{ct} / (k_{ri} + k_{ct})$, obtained from two series springs representing a pop-rivet k_{ri} and a cross tee connection k_{ct}. Assuming the mode shapes of beams with equally spaced elastic springs are unchanged by the presence of the springs (Blevins, 1979), the shape function is chosen as $\psi(x) = \sin(\pi x/L)$.

One of the analyses was performed using the input motion from a table impulse test of Test #12. The input motion was achieved at the center roof of the 6.3m × 6.3m test frame. The properties of the ceiling system are m = 0.16 lb-sec^2/ft^2, L = 12 ft. (distance between two lateral restraints), and EI = 82.6 kip-in^2. The spring stiffness k_s = 0.2 kip/in. The calculated fundamental frequency of the system is f_n = 13.9 Hz from the generalized mass and stiffness of Eqn. 5.3, while the measured frequency was 10.4 Hz estimated from the transfer function (the estimated ξ = 14%). It is noted that the analytical model represents a single main runner supported by the fixed side wall and lateral restraints as shown in Figure 5.3 while the measured acceleration was achieved from the middle main runner, which was neither supported by lateral restraints nor the fixed wall. The comparison between the experimental and analytical results of the main runner acceleration at $x = L/3$ is presented in Figure 5.4. The experiment shows also a contribution of a higher mode; however, both magnitude and vibrations are captured in analysis.

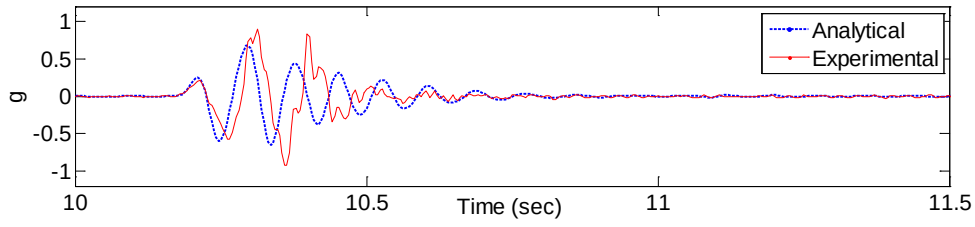

Figure 5.4. Comparison of acceleration histories from a table impulse test (Test #12)

6. REMARKS

For full scale shake table testing of suspended ceiling systems, a new test frame providing a continuous ceiling area up to 100m^2 and the open loop shake table compensation procedure was implemented. The combined designs of the physical frame and of the shake table motion controllers allowed simulating the required floor/roof motion according to ICC-ES AC156 at the roof structure, where the suspended ceiling system was attached. Fifteen different configurations were tested to investigate the effects of various assembly conditions. The basic lessons learned from the experiments are summarized as follows: i) The dynamic loads are collected by main runners from a tributary area of 1.22 m and transmitted to the end of the runners, or to lateral restraints (splay wires) in the longitudinal direction (along the main runner direction). Early failure of pop rivets was observed at the end of unrestrained runners. ii) The effects of lateral restraint were limited to the restrained runners only. No grid components provided enough lateral stiffness to transfer tributary loads from unrestrained runners to the restrainers. iii) The main runner deflection due to the dynamic forces in the transverse direction possibly caused cross tee connection failure. iv) Based on the fragility curves developed using the experimental data, it was learned that a ceiling system becomes more vulnerable when the system is excited by multi-directional input motions, when heavier tiles are used, when the ceiling area increases, and when lateral restraints are removed. Finally, new analytical models are developed based on the observation of the failure mechanisms in the longitudinal and transverse directions. The simple analytical models can represent the mechanics of the tested systems.

AKCNOWLEDGEMENT

The work is supported by the George E. Brown Network for Earthquake Engineering Simulation Grand Challenge (NEES-GC) research program of National Science Foundation, Grant Number NSF-CMMI-0721399. The authors acknowledge the contributions of the *practice and research committees* and of Armstrong Industries, Chicago Metallic Corp., and other ceilings and grid manufacturers participating in the program

REFERENCES

Reinhorn, A.M., Ryu, K.P. and Maddaloni, G. (2010). Modeling and Seismic Evaluation of Nonstructural Components: Testing Frame for Experimental Evaluation of Suspended Ceiling Systems, Technical Report MCEER -10-0004, NY.

MTS System Corporation. (2004). Real Time Hybrid Seismic Test System-User's Manual, USA.

ICC. (2010). ICC-ES AC156 Acceptance criteria for the seismic certification by shake-table testing of nonstructural components, International Code Council Evaluation Service, Whittier, California.

Maddaloni, G. , Ryu, K.P. and Reinhorn, A.M. (2010). Simulation of floor response spectra in shake table experiments. *Earthquake Engineering & Structural Dynamics*. **40:6**, 591–604.

Blevins, R.D. (1979). Formulas for Natural Frequency and Mode Shape, Van Nostrand Reinhold, NY.

Badillo, A.H. Whittaker, A.S. and Reinhorn, A.M. (2007). Seismic Fragility of Suspended Ceiling Sys-tems. *Earthquake Spectra*. **23:1**, 21–40.

Fenz, D.M. and Constantinou; M.C. (2008a). Mechanical Behavior of Multi-Spherical Sliding Bearings, Technical Report MCEER-08-0007, NY.

Reinhorn, A.M., Madan, A., Valles, R. E., Reichmann, Y., and Mander, J. B. (1995). Modeling of Masonary Infill Panels for Structural Analysis. Technical Report NCEER, NCEER-95-0018, NY.

Fenz, D.M. and Constantinou; M.C. (2008b). Development, Implementation and Verification of Dynamic Analysis Models for Multi-Spherical Sliding Bearings, Technical Report MCEER-08-0018, NY.

Chopra, A.K. (2007). Dynamics of Structures: Theory and Applications to Earthquake Engineering, 3rd Ed., Pearson Prentice-Hall: Upper Saddle River, NJ.